International Journal of Minerals, Metallurgy and Materials
Volume 29, Number 10, October 2022, Page 1901
https://doi.org/10.1007/s12613-022-2440-5

Hydrogen-based direct reduction of iron oxide at 700°C: Heterogeneity at pellet and microstructure scales

Yan Ma[1),✉], *Isnaldi R. Souza Filho*[1)], *Xue Zhang*[1,2)], *Supriya Nandy*[1)], *Pere Barriobero-Vila*[3)], *Guillermo Requena*[3,4)], *Dirk Vogel*[1)], *Michael Rohwerder*[1)], *Dirk Ponge*[1)], *Hauke Springer*[1,5)], *and Dierk Raabe*[1),✉]

1) Max-Planck-Institut für Eisenforschung, Max-Planck-Straße 1, 40237 Düsseldorf, Germany
2) Corrosion Center, Institute of Metal Research, Chinese Academy of Sciences, Shenyang 110016, China
3) Institute of Materials Research, German Aerospace Center (DLR), Linder Höhe, 51147 Cologne, Germany
4) Lehr- und Forschungsgebiet Metallische Strukturen und Werkstoffsysteme für die Luft- und Raumfahrt, RWTH Aachen University, 52062 Aachen, Germany
5) Institut für Bildsame Formgebung, RWTH Aachen University, Intzestraße 10, 52072 Aachen, Germany
(Received: 30 November 2021; revised: 24 January 2022; accepted: 15 February 2022)

Abstract: Steel production causes a third of all industrial CO_2 emissions due to the use of carbon-based substances as reductants for iron ores, making it a key driver of global warming. Therefore, research efforts aim to replace these reductants with sustainably produced hydrogen. Hydrogen-based direct reduction (HyDR) is an attractive processing technology, given that direct reduction (DR) furnaces are routinely operated in the steel industry but with CH_4 or CO as reductants. Hydrogen diffuses considerably faster through shaft-furnace pellet agglomerates than carbon-based reductants. However, the net reduction kinetics in HyDR remains extremely sluggish for high-quantity steel production, and the hydrogen consumption exceeds the stoichiometrically required amount substantially. Thus, the present study focused on the improved understanding of the influence of spatial gradients, morphology, and internal microstructures of ore pellets on reduction efficiency and metallization during HyDR. For this purpose, commercial DR pellets were investigated using synchrotron high-energy X-ray diffraction and electron microscopy in conjunction with electron backscatter diffraction and chemical probing. Revealing the interplay of different phases with internal interfaces, free surfaces, and associated nucleation and growth mechanisms provides a basis for developing tailored ore pellets that are highly suited for a fast and efficient HyDR.

Keywords: hydrogen-based direct reduction; iron oxide; microstructure; spatial gradient; metallization

1. Introduction

Steel is the dominant metallic alloy system, both in terms of quantity and breadth of applications, serving in transportation, civil and industrial infrastructures, construction, and safety. Steel also enables numerous clean energy and transport solutions, such as soft magnets in transformers, and structures and gears in huge wind power plants. More than 70% of the global raw iron production stems from blast furnaces (BFs), where CO is the major reductant [1]. The current annual consumption of iron ores for this process amounts to 2.3 billion tons, producing about 1.32 billion tons of pig iron [2], the historical name for the near eutectic iron–carbon alloy tapped from BFs. Each ton of steel produced through BFs and the subsequent basic oxygen furnace route creates about 1.9 t of CO_2 [3]. These numbers qualify iron- and steelmaking as the most staggering single sources of greenhouse gas on earth, accounting for 7%–8% of the global CO_2 emissions and ~35% of all CO_2 produced in the manufacturing sector [1]. The growth rate projections suggest a further massive increase in these emissions at least up to 2030 if no sustainable and disruptive technology changes are implemented [4–5]. These facts challenge current technology standards and operations, which are against the goals of achieving carbon-lean steel production and drastically reducing CO_2 emissions by more than 80% by 2050 [6–8]. Thus, iron- and steelmaking must be turned from one of the main culprits of global warming to key elements of a future sustainable and circular economy.

Thus, alternative reduction methods with potentially net-zero emissions for the extraction of iron from its ores have to be urgently studied, identified, matured, and implemented based on a thorough understanding of the underlying physical and chemical mechanisms. Several strategies, including a variety of solid, molecular, ionic, proton, or electron-based reductants, are conceivable, and the associated synthesis and reduction methods, in part, can be combined (Fig. 1). An alternative approach for large-scale and sustainable iron oxide

✉ Corresponding authors: Dierk Raabe E-mail: d.raabe@mpie.de; Yan Ma E-mail: y.ma@mpie.de

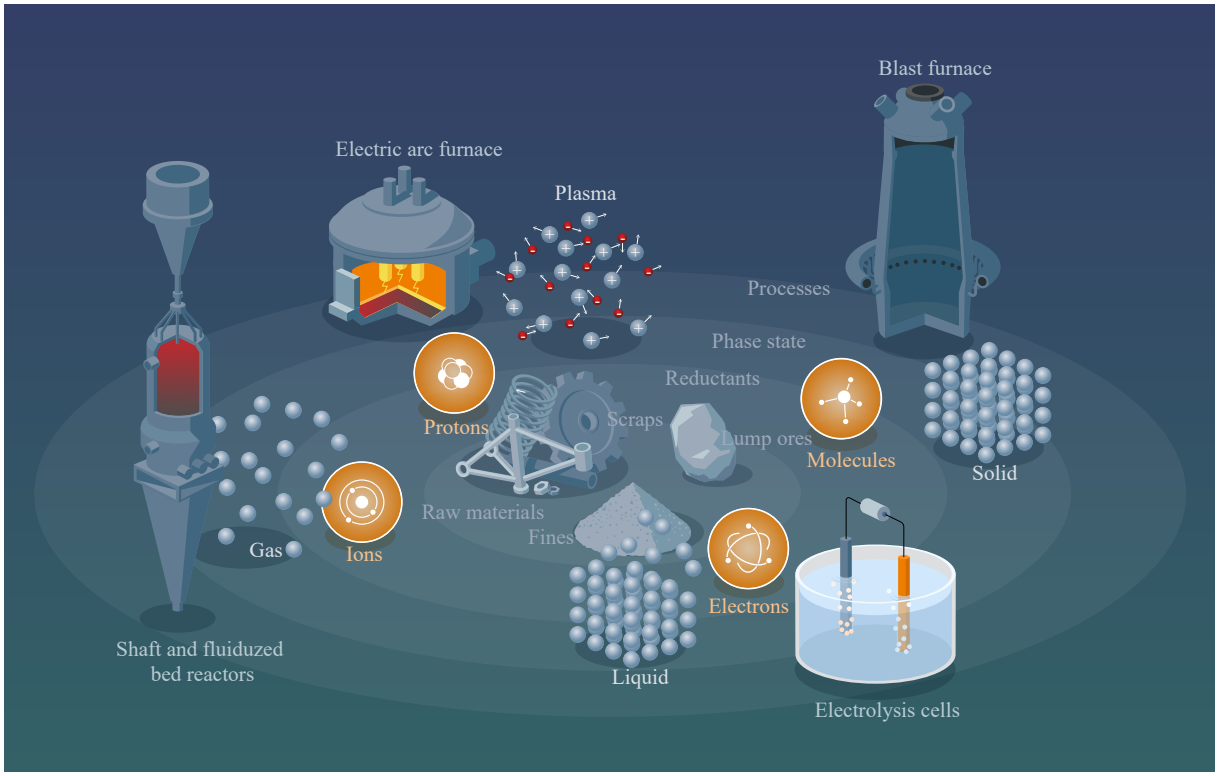

Fig. 1. Pathways and combinations for melting scraps and reducing iron oxide lump ores, pellets, or fines that are conceivable when using a wide range of reductants and aggregate states.

reduction is the use of hydrogen gas, its carriers [9], and their plasma variants [10], provided that reducing agents (instead of carbon) originate from sustainable or low-carbon sources [11]. In particular, the current study addressed hydrogen-based direct reduction (HyDR) with molecular hydrogen.

The HyDR involves multiple phase transformations [11–12]. At temperatures above 570°C, HyDR proceeds along the sequence Fe_2O_3 (hematite) → Fe_3O_4 (magnetite) → $Fe_{(1-x)}O$ (wüstite) → α-Fe (BCC iron) or γ-Fe (FCC iron). Meanwhile, at temperatures below 570°C, wüstite is no longer thermodynamically stable, and the reduction reaction proceeds in the order Fe_2O_3 → Fe_3O_4 → α-Fe. The overall reaction is endothermic when using H_2 as the reductant. Several investigations addressed the use of H_2 as a reductant [13–16]. These studies focused on the global reduction thermodynamics, kinetics, and the effect of process parameters (e.g., gas flow rate, temperature, and pressure) rather than on the microscopic nucleation and growth mechanisms or gradients of these features through feedstock dimensions [17–23]. Pineau *et al.* studied the reduction of hematite and magnetite [19–20]. The latter is an interesting option, given that magnetite ores can become a commercially attractive alternative feedstock when new furnace types and reduction methods enter the market. In addition, their findings indicated that the reaction rate was controlled by the growth of nuclei and phase boundary reactions. Piotrowski *et al.* [24–25] studied the reduction kinetics of hematite to magnetite and wüstite using thermogravimetry and described the kinetics using a classical Avrami nucleation and growth model. Patisson's group [4,26] developed detailed models of the mesoscale structure of the feedstock material, accounting for the role of the granularity of pellets. Bonalde *et al.* [27] studied the reduction of Fe_2O_3 pellets with high inherited porosity and exposed to gas mixtures of H_2 and CO. They concluded that the interface reactions and oxygen diffusion acted as competing processes during the first reduction stage and the internal gas diffusion as a rate-controlling step during the last stage. One assumption of their model was that the phase boundary moved toward the center of pellets and that the oxide feedstock material had neither porosity nor delamination cracks. However, this assumption does not fully agree with the findings reported in the recent literature [9]. Hence, considering more details about the pellet defect structures (such as interfaces, cracks, pores, and dislocations) at the microscopic scale and their spatial gradient at the mesoscopic scale is important to understand the reduction kinetics and metal yield [4].

The present investigation aimed to gain further insights into the influence of pellet morphology and its internal microstructure on the overall reduction efficiency and metallization. For this purpose, commercial direct reduction (DR) pellets were investigated using synchrotron high-energy X-ray diffraction (HEXRD) and scanning electron microscopy in conjunction with electron backscatter diffraction (EBSD) and energy-dispersive X-ray spectroscopy (EDX). This approach revealed the microstructural morphology and spatial gradients of the phase transformations during the HyDR and the interplay of different phases with the internal interfaces. The obtained results can guide the development of next-generation reactors and pellet feedstock that are better suited for a fast and efficient HyDR to make ironmaking affordably carbon free.

2. Experimental

We investigated the role of pellet morphology and microstructure in the reduction kinetics of the last and most important stage, i.e., from wüstite to iron. A special emphasis was placed on the quantitative mapping of the heterogeneity of reduction and radial gradients in the reduction kinetics of a partially reduced pellet. For this purpose, we used the same commercial DR hematite pellets as in a preceding study [9]. The pellet had a diameter of about 11 mm and a chemical composition of 0.36wt% FeO, 1.06wt% SiO_2, 0.40wt% Al_2O_3, 0.73wt% CaO, 0.57wt% MgO, 0.19wt% TiO_2, 0.23wt% V, 0.10wt% Mn, and Fe_2O_3 in balance. The pellet also contained traces of P, S, Na, K, V, and Ti. The pellet was isothermally exposed to pure hydrogen with a constant flow rate of 0.5 L/min at 700°C in a thermogravimetric configuration [28]. The mass loss of the pellet was continuously monitored by the thermal balance during the reduction experiment. The reduction degree R was determined from the experimental mass loss divided by the theoretical mass loss, with the hematite in the pellet considered to be fully reduced into iron.

The phase distribution along the radius of the partially reduced pellet was characterized by synchrotron HEXRD. For this purpose, a disk sample with a thickness of ~2 mm was sliced from the center of the spherical pellet using a diamond wire saw. HEXRD measurements were conducted in transmission mode at the beamline P07 (High Energy Materials Science) of PETRA III in Deutsches Elektronen-Synchrotron. The beamline was operated with a fixed beam energy of ~100 keV, and the corresponding wavelength of the X-ray beam was 0.0124 nm. The probing beam size was 0.5 mm × 0.5 mm. The Debye–Scherrer diffraction rings were recorded by an area detector (PerkinElmer XRD1621USA) and integrated by the Fit2D software [29]. The phase fraction was calculated based on the Rietveld refinement method using the MAUD software [30]. The local microstructure was further analyzed using secondary electron imaging, EBSD, and correlative EDX in scanning electron microscopy (SEM). The step size for EBSD measurement was 50 nm. The acquired EBSD and EDX data were analyzed using the OIM Analysis™ V8.6 software package.

3. Results

3.1. Kinetics of DR of hematite pellet at 700°C under hydrogen atmosphere

Fig. 2 presents the experimentally observed reduction kinetics in terms of the reduction degree for the HyDR of commercial hematite pellets. The data are comparable to those shown in our preceding work [9] and the results of other groups [4,21]. The reduction rates of the first two reduction steps, i.e., from hematite (Fe_2O_3) to magnetite (Fe_3O_4) and from magnetite to wüstite ($Fe_{(1-x)}O$), were high at about 0.5×10^{-3}–1.8×10^{-3} s^{-1} (Fig. 2(b)). The wüstite reduction to α-iron (α-Fe) started considerably slow, at about 0.6×10^{-3} s^{-1}, and slowed down continuously toward the end of the redox reaction. The reduction degree reached 95% after the reduction for about 37 min and 98% after 52 min, indicating that the reduction in this stage was extremely sluggish, and complete metallization was not fully obtained. The analysis and discussion of the individual kinetic steps and the roles of some of the underlying microstructures, nucleation, transport, and growth mechanisms have been recently studied by using SEM and atom probe tomography [9] and will thus not be repeated in detail here.

The most common feature of all these sequential phase transformation steps during this redox reaction is the gradual deceleration of the transformation rate during the transformation within the same phase regime. An important reason for this was discovered in the pellet microstructure. During the early stages of individual phase transformations, the material showed a very rich density of lattice defects, in particular high porosity (due to the gradual mass loss), delamination at

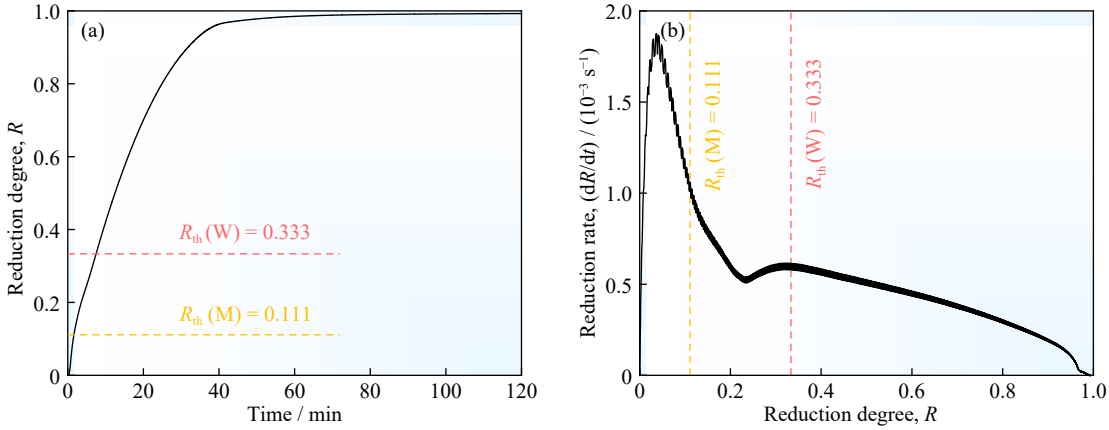

Fig. 2. (a) Reduction degree in terms of mass change as a function of time and (b) reduction rate (that is, the first derivative of the reduction degree) as a function of reduction degree for a commercial DR hematite pellet. Reduction in a static bed was conducted under pure hydrogen gas at a flow rate of 0.5 L/min at 700°C. The dotted marker line R_{th}(M) at the reduction degree of 0.111 indicates the theoretically expected reduction from hematite to magnetite, and line R_{th}(W) at 0.333 denotes the one from magnetite to wüstite, according to the stoichiometry of the phases. The specimen studied here for radial-gradient effects was obtained after an exposure duration of 30 min.

the hetero-interfaces, and cracking (due to the high-volume mismatch between the adjacent phases and the resulting mechanical stresses). Another important aspect was that the pellets contained a high-volume fraction of inherited pores. This feature facilitated rapid outbound mass transport (of oxygen) and the removal of water from these surface reaction fronts. Thus, rapid nucleation and growth were always enabled close to these internal free surfaces, specifically at the beginning of the reduction. However, with further progress of the reaction, the remaining oxide regions became increasingly surrounded by the reduction products. As the remaining volume became smaller and highly dispersed, considerably fewer lattice defects were directly connected to them as pathways for rapid diffusion. Thus, toward the end of these reduction steps, the small remaining oxide regions were less frequently in contact with delamination and cracking features. The remaining oxide regions were surrounded by denser reaction products that impeded oxygen removal.

3.2. Through-pellet heterogeneity of microstructures during HyDR at 700°C

Fig. 3 presents an overview of the main differences in the microstructure, phase composition, and porosity probed by SEM and HEXRD along the radius of a hematite pellet that was reduced with hydrogen at 700°C after an exposure period of 30 min. The results revealed a gradient in microstructure, porosity, and phases between the near-surface and interior regions of the pellet.

The pellets are granular agglomerates consisting of sintered polycrystalline substructure units that are hierarchically stacked together with large pore regions among them (e.g., the visible pores in Fig. 3(a) and the large pores among the sintered substructure units in Fig. 3(b)–(d)). These general aspects of pellet morphology, the granular substructure, and their role on reduction kinetics were studied in detail in the papers of Patisson's group [4,31–32] and Kim *et al.* [9]. In the near-surface regions of the pellets, oxygen can rapidly diffuse outbound either toward the outer free surface of the pellet or the adjacent free volume in the form of pores that were inherited from the pelletizing process. On these free surfaces, oxygen can combine with hydrogen to form water.

Another kinetically relevant factor is that hydrogen intrudes from the outer free pellet surfaces, and as a result, the outer regions are naturally the ones reduced most rapidly.

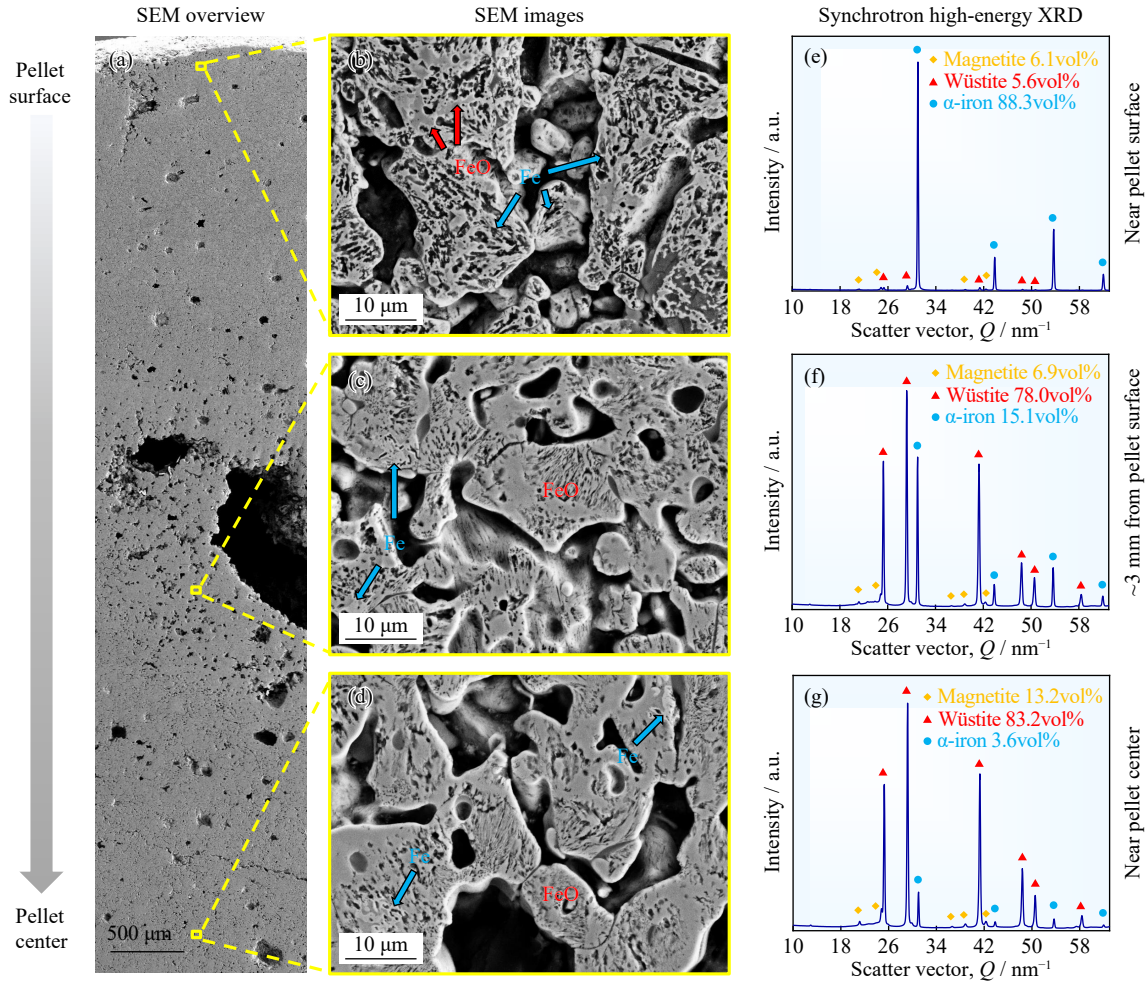

Fig. 3. Overview of the microstructure, phase fractions, and porosity along the radius of a hematite pellet reduced at 700°C for 30 min with pure hydrogen, probed by SEM and synchrotron HEXRD. (a) SEM overview of the pellet structure between the surface and center regions. Magnified SEM images of the microstructures in (b) the near-surface region, (c) the region ~3 mm below the surface, and (d) the center region of the pellet. (e–f) Bulk HEXRD analysis of the spatial distribution of phase constituents along the pellet radius (probing volume of 0.5 mm × 0.5 mm × 2 mm).

This basic kinetic scenario is supported by the microstructure gradient along the pellet radius quantitatively measured by HEXRD (Fig. 3). The surface area of the pellet revealed the highest metallization degree of 88.3vol% α-iron, with the remaining small fractions consisting of wüstite (5.6vol%) and magnetite (6.1vol%). Conversely, the metallization dropped to 15.1vol% α-iron in the region about 3 mm below the pellet surface, with large portions of the remaining iron oxides, *i.e.*, 78.0vol% wüstite and 6.9vol% magnetite. No significant difference was observed in the phase fractions in the center region of the pellet (83.2vol% wüstite, 13.2vol% magnetite, and 3.6vol% α-iron) compared with the region about 3 mm below the pellet surface. This HEXRD result indicated a very drastic difference in the reduction rate between the near-surface regions of the pellet and its interiors.

3.3. Local microstructure

Fig. 4 shows the microstructure and phase topology in a region about 2 mm below the surface of the partially reduced pellet (within the topochemical interface of the FeO → Fe transition). The reduced iron was visible in these backscattered electron (BSE) images due to its bright contrast, whereas wüstite appeared in a darker gray contrast. The black regions are the pores that were inherited from pellet sintering (between iron or oxide particles) and formed due to mass loss during the reduction process (within iron or oxide particles). The important microstructure features at this last reduction stage (i.e., from wüstite to iron) will be discussed in this section.

The micrographs shown in Fig. 4 revealed several fundamental features that are characteristics of the entire HyDR process when using such pellets. One important feature was that all of the iron formed adjacent to the free surfaces. This feature matched the kinetic expectations regarding the fast hydrogen intrusion due to gaseous surface diffusion along these free volume regions and the fast removal rate of oxygen at the internal interfaces, where water was formed and stored. At the beginning of the reduction, hydrogen ingress, oxygen removal, and the recombination of the hydrogen and oxygen into water occurred only in the large percolating pore regions inherited from the pelletizing process. However, several of these pores evolved during the gradual removal of oxygen during the reduction. This phenomenon can be observed in terms of the evolving nanoscale porosity inside the wüstite region (Fig. 4(b)). With the ongoing gradual removal of oxygen, these pores further grew and locally recombined into larger ones over the course of the reduction.

The nucleation barrier for the formation of iron is also likely smaller on the free surface than in the interior. This condition is due to (1) the heterogeneous nucleation advantage, in which a portion of the required interface energy is already provided by these inner open surfaces and (2) the relaxation of elastic stresses upon iron nucleation on the surface. Owing to the large volume difference between iron and wüstite (more than 40%) [33], the latter aspect was assumed to have a substantial energetic influence on the nucleation barrier. When considering the associated elastic misfit stresses in the calculation of the required nucleation energies (which is expected in the gigapascal range if no plastic relaxation occurs) [34], the surface nucleation barriers for forming iron are substantially lower than those in the interior.

Another important microstructure feature is that some of the remaining inner wüstite regions became increasingly encapsulated by iron. A limited number of delamination features and pores were observed at the hetero-interfaces (Fig. 4). This behavior was also revealed by the phase and composition maps shown in Fig. 5. The consequence of this composite phase topology is that the outbound oxygen transport must proceed through the surrounding bulk iron regions. As a result, the last reduction stages were relatively slow, and the reduction rate continuously dropped (Fig. 2) [9]. Such a microscopic core-shell behavior was different from the reduction behavior in the early stage of wüstite to iron transition, in which numerous delamination features were observed at the wüstite/iron hetero-interfaces [9].

4. Discussion

The results revealed a large difference in the reduction rate and metallization along the pellet radius. This observation raises concerns not only regarding the overall sluggish reduction rate due to these gradient effects but also the low efficiency obtained with the use of hydrogen. The decarbonization of the global steel industry with the aid of techniques, such as the HyDR, is reasonable only when green hydrogen is used. This aspect means that the beneficial total efficiency and life-cycle assessment regarding the carbon footprint re-

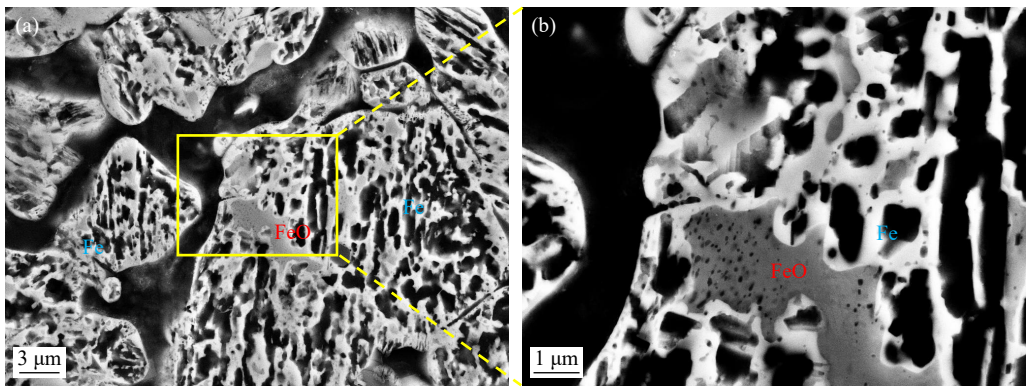

Fig. 4. BSE images captured at high magnification, revealing the local distribution of pores, wüstite, and iron in the region about 2 mm below the pellet surface after reduction at 700°C for 30 min with pure hydrogen.

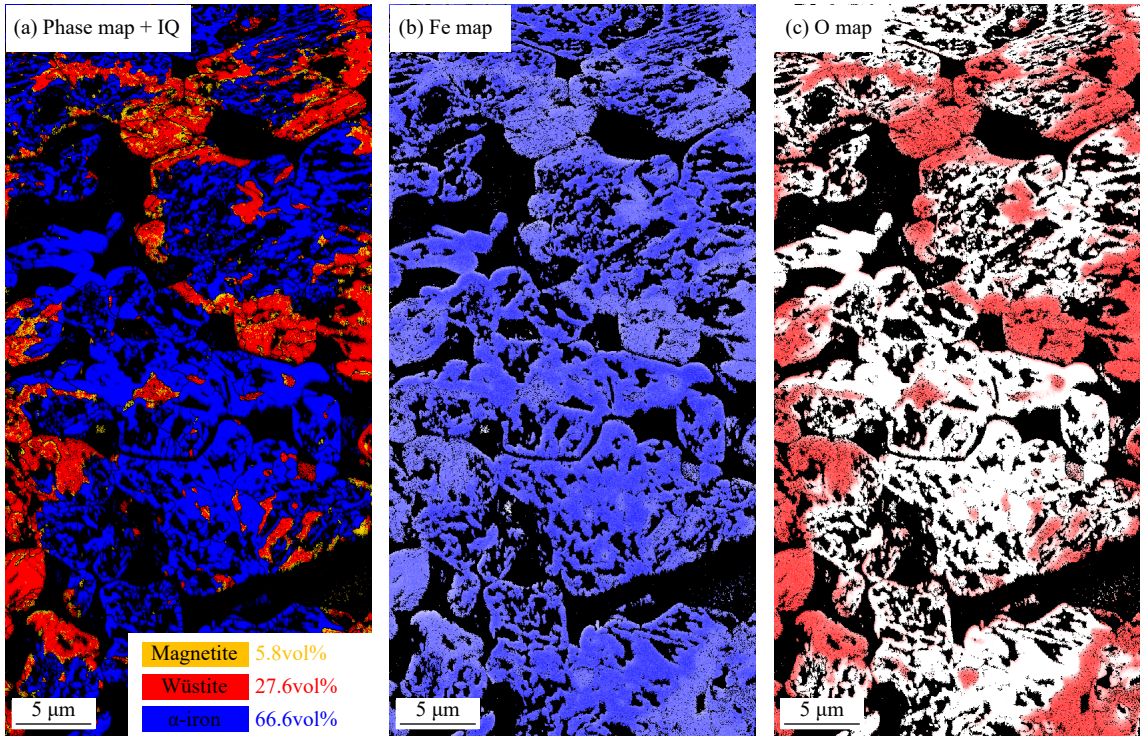

Fig. 5. Local phase and elemental distribution in the region about 2 mm below the surface of the partially reduced pellet probed by EBSD and EDX: (a) EBSD phase map imposed on image quality (IQ); (b) iron and (c) oxygen distribution maps.

quire hydrogen produced by sustainable energy sources, making it a very expensive product. Thus, hydrogen should be used in such reduction processes as efficiently as possible. In addition, an assessment of the total efficiency of the HyDR processes requires not only the consideration of the total energy balance but also the total efficiency of hydrogen consumption as an essential cost and sustainability factor.

The large through-pellet gradient of reduction kinetics observed in this study suggests the reconsideration of the suitability of the current commercial pellet design or process optimization for HyDR processes. In particular, given the unique physical properties of molecular hydrogen, i.e., its smaller molecular size and lower viscosity compared with CO or CH_4, the gas transport phenomena in the HyDR can be very different from those in processes with carbon-based reductants. Thus, further studies will be performed to assess experimentally and theoretically the effect of pellet size, porosity, and microstructure on the gaseous percolation. In this case, the improved characterization of porous structures is highly needed to reveal the three-dimensional connectivity of pores. This information is important to disentangle the percolation paths. With the further help of fluid dynamic simulation, the underlying gas transport phenomena can be better understood. The gained knowledge will allow for the knowledge-based pellet design, which will enable the acceleration of the overall reduction kinetics in HyDR processes.

5. Conclusion and outlook

In this study, we quantitatively investigated the spatial gradient of the microstructure of a partially reduced commercial hematite pellet and its influence on reduction kinetics during the HyDR. The microstructural analysis along the pellet radius revealed the strong heterogeneity of the reduction rate. The surface region of the pellet showed a high metallization of 88vol% α-iron, whereas the center region of the pellet contained about 4vol% α-iron. The local microstructural analysis further suggested that the outbound diffusion of oxygen was substantially delayed not only in the center areas of the pellets but also in the sub-surface zones because the remaining wüstite islands were encapsulated by iron. In addition, the observed abundance of defect-mediated transport pathways for fast oxygen diffusion is insufficient to warrant more homogeneous and rapid reduction kinetics. Further experimental and fluid dynamic simulations should be conducted to better understand the effect of pellet size, porosity, and microstructure on gaseous percolation. The current findings can provide guidance for the optimization of pellets in terms of size, porosity, and microstructure to meet the demands of fast and efficient HyDR.

Acknowledgements

Y. Ma acknowledges the financial support from the Walter Benjamin Programme of the Deutsche Forschungsgemeinschaft (No. 468209039). I.R. Souza Filho acknowledges the financial support from Capes-Humboldt (No. 88881.512949/2020-01). H. Springer acknowledges the financial support from the Heisenberg Programme of the Deutsche Forschungsgemeinschaft (SP 1666 2/1). The authors would like to acknowledge the support provided by N. Schell and A. Stark (Helmholtz-Zentrum Hereon) for the high-energy X-ray diffraction experiments at the P07 High Energy Materials Science beamline. The Deutsches

Elektronen-Synchrotron (DESY) is acknowledged for the provision of synchrotron radiation facilities in the framework of proposal I-20191042.

Conflict of Interest

The authors declare that they have no known competing financial interests or personal relationships that could have appeared to influence the work reported in this paper.

Open Access funding enabled and organized by Projekt DEAL.

References

[1] D. Raabe, C.C. Tasan and E.A. Olivetti, Strategies for improving the sustainability of structural metals, *Nature*, 575(2019), No. 7781, p. 64.

[2] World Steel Association, *World Steel in Figures 2021* [2022-01-24]. https://worldsteel.org/wp-content/uploads/2021-World-Steel-in-Figures.pdf

[3] M. Flores-Granobles and M. Saeys, Minimizing CO_2 emissions with renewable energy: A comparative study of emerging technologies in the steel industry, *Energy Environ. Sci.*, 13(2020), No. 7, p. 1923.

[4] F. Patisson and O. Mirgaux, Hydrogen ironmaking: How it works, *Metals*, 10(2020), No. 7, p. 922.

[5] W. Jaimes and S. Maroufi, Sustainability in steelmaking, *Curr. Opin. Green Sustainable Chem.*, 24(2020), p. 42.

[6] M. Pei, M. Petäjäniemi, A. Regnell, and O. Wijk, Toward a fossil free future with HYBRIT: Development of iron and steelmaking technology in Sweden and Finland, *Metals*, 10(2020), No. 7, p. 972.

[7] S. Lechtenböhmer, C. Schneider, M. Yetano Roche, and S. Höller, Re-industrialisation and low-carbon economy—Can they go together? Results from stakeholder-based scenarios for energy-intensive industries in the German state of north Rhine Westphalia *Energies*, 8(2015), No. 10, p. 11404.

[8] M. Fischedick, J. Marzinkowski, P. Winzer, and M. Weigel, Techno-economic evaluation of innovative steel production technologies, *J. Clean. Prod.*, 84(2014), p. 563.

[9] S.H. Kim, X. Zhang, Y. Ma, *et al.*, Influence of microstructure and atomic-scale chemistry on the direct reduction of iron ore with hydrogen at 700°C, *Acta Mater.*, 212(2021), p. 116933.

[10] I.R. Souza Filho, Y. Ma, M. Kulse, *et al.*, Sustainable steel through hydrogen plasma reduction of iron ore: Process, kinetics, microstructure, chemistry, *Acta Mater.*, 213(2021), p. 116971.

[11] D. Spreitzer and J. Schenk, Reduction of iron oxides with hydrogen—A review, *Steel Res. Int.*, 90(2019), No. 10, p. 1900108.

[12] Y. Ma, I.R. Souza Filho, Y. Bai, *et al.*, Hierarchical nature of hydrogen-based direct reduction of iron oxides, *Scripta Mater.*, 213(2022), p. 114571.

[13] E.T. Turkdogan and J.V. Vinters, Gaseous reduction of iron oxides: Part I. Reduction of hematite in hydrogen, *Metall. Mater. Trans. B*, 2(1971), No. 11, p. 3175.

[14] M.V.C. Sastri, R.P. Viswanath, and B. Viswanathan, Studies on the reduction of iron oxide with hydrogen, *Int. J. Hydrogen Energy*, 7(1982), No. 12, p. 951.

[15] H.Y. Lin, Y.W. Chen, and C. Li, The mechanism of reduction of iron oxide by hydrogen, *Thermochim. Acta*, 400(2003), No. 1-2, p. 61.

[16] M. Moukassi, P. Steinmetz, B. Dupre, and C. Gleitzer, A study of the mechanism of reduction with hydrogen of pure wustite single crystals, *Metall. Trans. B*, 14(1983), No. 1, p. 125.

[17] M.J. Tiernan, P.A. Barnes, and G.M.B. Parkes, Reduction of iron oxide catalysts: The investigation of kinetic parameters using rate perturbation and linear heating thermoanalytical techniques, *J. Phys. Chem. B*, 105(2001), No. 1, p. 220.

[18] J. Zieliński, I. Zglinicka, L. Znak, and Z. Kaszkur, Reduction of Fe_2O_3 with hydrogen, *Appl. Catal. A Gen.*, 381(2010), No. 1-2, p. 191.

[19] A. Pineau, N. Kanari, and I. Gaballah, Kinetics of reduction of iron oxides by H_2: Part I: Low temperature reduction of hematite, *Thermochim. Acta*, 447(2006), No. 1, p. 89.

[20] A. Pineau, N. Kanari, and I. Gaballah, Kinetics of reduction of iron oxides by H_2: Part II: Low temperature reduction of hematite, *Thermochim. Acta*, 456(2007), No. 2, p. 75.

[21] H.B. Zuo, C. Wang, J.J. Dong, K.X. Jiao, and R.S. Xu, Reduction kinetics of iron oxide pellets with H_2 and CO mixtures, *Int. J. Miner. Metall. Mater.*, 22(2015), No. 7, p. 688.

[22] Q.T. Tsay, W.H. Ray, and J. Szekely, The modeling of hematite reduction with hydrogen plus carbon monoxide mixtures: Part I. The behavior of single pellets, *AIChE J.*, 22(1976), No. 6, p. 1064.

[23] E. Kawasaki, J. Sanscrainte, and T.J. Walsh, Kinetics of reduction of iron oxide with carbon monoxide and hydrogen, *AIChE J.*, 8(1962), No. 1, p. 48.

[24] K. Piotrowski, K. Mondal, H. Lorethova, L. Stonawski, T. Szymański, and T. Wiltowski, Effect of gas composition on the kinetics of iron oxide reduction in a hydrogen production process, *Int. J. Hydrogen Energy*, 30(2005), No. 15, p. 1543.

[25] K. Piotrowski, K. Mondal, T. Wiltowski, P. Dydo, and G. Rizeg, Topochemical approach of kinetics of the reduction of hematite to wüstite, *Chem. Eng. J.*, 131(2007), No. 1-3, p. 73.

[26] H. Hamadeh, O. Mirgaux, and F. Patisson, Detailed modeling of the direct reduction of iron ore in a shaft furnace, *Materials* (*Basel*), 11(2018), No. 10, art. No. 1865.

[27] A. Bonalde, A. Henriquez, and M. Manrique, Kinetic analysis of the iron oxide reduction using hydrogen-carbon monoxide mixtures as reducing agent, *ISIJ Int.*, 45(2005), No. 9, p. 1255.

[28] M. Auinger, D. Vogel, A. Vogel, M. Spiegel, and M. Rohwerder, A novel laboratory set-up for investigating surface and interface reactions during short term annealing cycles at high temperatures, *Rev. Sci. Instrum.*, 84(2013), No. 8, p. 085108.

[29] A.P. Hammersley, FIT2D: A multi-purpose data reduction, analysis and visualization program, *J. Appl. Crystallogr.*, 49(2016), No. 2, p. 646.

[30] L. Lutterotti, Total pattern fitting for the combined size-strain-stress-texture determination in thin film diffraction, *Nucl. Instrum. Methods Phys. Res., Sect. B*, 268(2010), No. 3-4, p. 334.

[31] A. Ranzani da Costa, D. Wagner, and F. Patisson, Modelling a new, low CO_2 emissions, hydrogen steelmaking process, *J. Clean. Prod.*, 46(2013), p. 27.

[32] D. Wagner, O. Devisme, F. Patisson, and D. Ablitzer, A laboratory study of the reduction of iron oxides by hydrogen, [in] F. Kongoli and R.G. Reddy, eds., *Proceedings of Sohn International Symposium*, San Diego, 2006, p. 111.

[33] W.C. Mao and W.G. Sloof, Reduction kinetics of wüstite scale on pure iron and steel sheets in Ar and H_2 gas mixture, *Metall. Mater. Trans. B*, 48(2017), No. 5, p. 2707.

[34] Y. Bai, J. R. Mianroodi, Y. Ma, A.K. da Silva, B. Svendsen, and D. Raabe, Chemo-mechanical phase-field modeling of iron oxide reduction with hydrogen, *Acta Mater.*, 231(2022), p. 117899.